Journal of Electromagnetic Waves and Applications, Vol. 8, No. 4, 509–529, 1994

Finite-difference time-domain formulation of an inverse scattering scheme for remote sensing of conducting and dielectric targets: Part II - Two dimensional case

M. Strickel

Rand Financial Services
141 N. Jackson Blvd.
Chicago, Illinois 60604, USA

A. Taflove

Department of Electrical Engineering and Computer Science
Northwestern University
Evanston, Illinois 60208, USA

K. Umashankar

Department of Electrical Engineering and Computer Science
University of Illinois at Chicago
Chicago, Illinois 60680, USA

Abstract–This paper introduces a technique for time-domain electromagnetic inverse scattering based upon the use of a two-dimensional, finite-difference time-domain (FD-TD) forward scattering field representation in numerical feedback loop with a nonlinear optimization routine. Causality is exploited to reconstruct the actual target surface contour in a sequential and cumulative manner as the illuminating wavefront sweeps across the target. This approach appears to require a minimum amount of scattered field information. A number of examples are reported where the only data needed is the time waveform of a scattered pulse for the transverse magnetic (TM) polarization case, observed at just a single point in the near field. These examples include the reconstruction of two-dimensional conducting and homogeneous dielectric target shapes such as triangles, rectangles, and trapezoids. A dielectric target with reentrant features, resembling the letter "J" is also reconstructed from a single point observation. The effects of measurement signal-to-noise ratio upon this inverse-scattering technique are determined via numerical experiments. These effects are discussed in two contexts: 1) probability of exact reconstruction vs. signal-to-noise ratio, and 2) sensitivity of reconstructions to noise. It is shown that, even at low signal-to-noise ratios (where the probability of exact reconstruction is also low), the imperfectly-reconstructed targets retain many of the distinguishing features of the original target. This indicates that the reconstruction process is quite robust relative to noise. Developments in nonlinear optimization appear promising for further improving the reliability and quality of target reconstruction in noise.

I. INTRODUCTION

In this paper, we introduce a technique for time-domain electromagnetic inverse scattering based upon the use of a two-dimensional, finite-difference time-domain

(FD-TD) forward scattering field representation in a numerical feedback loop with a nonlinear optimization routine. This technique is presently aimed at reconstruction of the shapes of two-dimensional targets of known dielectric permittivity and conductivity, assuming homogeneity of the dielectric parameters. A key goal is to achieve target shape reconstruction using a minimum of scattered field information. In the examples reported here, the only data required is the time waveform of a scattered pulse for the TM polarization case, observed at just a single point in the near field. The ability to reconstruct target shapes from a minimum amount of data is made possible by exploiting causality. Causality permits target shape reconstruction to proceed sequentially in time as the illuminating wavefront sweeps across the target. Sequential, cumulative target reconstruction in this manner is a characteristic of time-domain inverse scattering, in general, relative to frequency-domain approaches.

The technique reported here is an extension of the one-dimensional electromagnetic profile inversion method reported by Umashankar, et. al. [1,2]. Their approach combines a one-dimensional, forward-scattering, FD-TD code in a numerical feedback loop with an unconstrained nonlinear optimization routine. Using this technique, references [1,2] report reconstruction of arbitrary, spatially-coincident profiles of electrical permittivity and conductivity.

The technique of combining a forward-scattering FD-TD field representation with a nonlinear optimization routine has also been applied recently to nonlinear inversion of acoustic and seismic waveforms. For example, Fawcett [3] applies a finite-difference time-domain representation of the acoustic wave equation with nonlinear optimization based on least squares and the Lovenberg-Marquardt solution method to two-dimensional inverse problems in acoustics. Using this model, Fawcett estimates the acoustic velocity distribution of a medium in a finite rectangular domain. The medium is excited by a point source of known location, and measured data consists of the scattered fields observed along one edge of the domain. Gauthier, Virieux, and Tarantola [4] use a time-domain, velocity-stress, finite-difference method to first solve the forward problem of calculating seismograms. The inversion of the seismic waveforms is then formulated as a least-squares minimization problem which is iteratively solved using a gradient method. This method is used to obtain the unknown bulk modulus of a circular inclusion in a homogeneous medium. A variety of source-receiver configurations are reported, including 8 sources and 100 receivers arranged in a straight line, and 8 sources and 400 receivers placed all around the inclusion.

Although the FD-TD/feedback method has been recently applied to acoustic and seismic inverse problems, this paper appears to be the first multi-dimensional application of this technique to target-shape reconstruction in electromagnetics. Previous research in time-domain target-shape reconstruction is formulated in terms of integral equations. For example, Bennett [5] uses an exact space-time integral equation to reconstruct rotationally symmetric, perfectly conducting, three-dimensional targets. A number of other workers have applied integral equations to time-domain inverse problems in one-dimension [6,7]. However, the time-domain integral equation approach has substantial limitations which are not shared by the FD-TD/feedback technique. One limitation is that the integral equation representation requires a time-dependent Green's function. This function is difficult to obtain if volume integration is required in a medium which is dispersive, inhomogeneous, or anisotropic. Another limitation is the requirement for back storage in time, which in combination with the requirement for sampling the unknown induced surface currents as a function of position, places serious restrictions on the size and dimensionality of the problem that can be modeled [8].

This paper reports two FD-TD/feedback algorithms which allow the reconstruction of two-dimensional target shapes from the near-field scattered pulse response. The first approach is a contour-following method that reconstructs the boundary of a convex conducting target as a series of straight line segments, where each new segment is connected to the tip of the previously constructed segment. Contour following is simple to implement and easily copes with causality locus distortion. However, contour following is difficult to apply to the reconstruction of targets having reentrant features. For such targets, we introduce a second method which reconstructs the target as a series of layers, where the position of each layer is determined by a simple gradient method. For both approaches, reconstruction is achieved using limited input data which consists of only the scattered electric field time waveform observed at a single point.

II. BACKGROUND OF THE BASIC FD-TD METHOD

In the mid 1960's, Yee introduced a computationally efficient means of directly solving Maxwell's time-dependent curl equations using finite differences [9]. With this approach, the continuous electromagnetic field in a finite volume of space is sampled as distinct points in a space lattice and at distinct equal-spaced points in time. Wave propagation, scattering, and penetration phenomena are modeled in a self-consistent manner by marching in time, that is, repeatedly implementing the finite-difference analog of the curl equations at each lattice point. This results in a simulation of the continuous actual waves by sampled data numerical analogs propagating in a data space stored in a computer. Space and time sampling increments are selected to avoid aliasing of the continuous field distribution, and to guarantee stability of the time-marching algorithm. Time marching is completed when the desired late-time or sinusoidal steady-state field behaviour is observed.

The Yee formulation, designated as the finite-difference time-domain (FD-TD) method, permits in principle the modeling of electromagnetic wave interactions with a level of detail comparable to that of the method of moments. Further, the explicit nature of the Yee algorithm leads to overall computer storage and running time requirements for FD-TD that are linearly proportional to N, the number of field unknowns in the finite volume of space being modeled for non-resonant structures spinning approximately 0.1 to 30 wavelengths. However, the use of FD-TD was very limited until the early 1980's because of a number of basic problems. The most important problem was that Yee's formulation provided for no simulation of the field sampling space extending to infinity. This deficiency caused spurious, non-physical reflection of the numerical wave analogs at the outermost planes of the space lattice. A second key problem was that Yee's formulation provided for no simulation of an incident wave having an arbitrary duration, angle of incidence, or angle of polarization. And third, the volumetric space discretization required by FD-TD caused its computer resource needs to seem prohibitive.

By the mid 1980, the major difficulties with FD-TD were largely overcome. Building on basic research in one-way wave equations and high-order expansions for radiation conditions [10,11], a numerical radiation boundary condition was formulated [12] which accurately simulates the extension of the FD-TD field sampling space to infinity. An accurate simulation of an incident wave of arbitrary duration, pulse shape, angle of incidence, and angle of polarization was reported independently in [12,13]. This was accomplished by zoning the FD-TD lattice into a total-field region (in which the structure of interest is embedded) surrounded by a scattered-field region, and providing a proper connecting condition between the regions. Finally, evolving computer hardware and software technology provided means to satisfy FD-TD requirements in central memory size, arithmetic speed, and bandwidth to high-speed secondary memory to enable routine usage of FD-TD for modeling three-dimensional structures containing more than 10^6 unknown electromagnetic field components in less than 10 minutes per illumination angle [14]. Detailed FD-TD/inverse scattering algorithm along with two-dimensional reconstruction examples are presented in the following.

III. BASIC FD-TD/FEEDBACK INVERSE SCATTERING ALGORITHM

Figure 1 shows a block diagram of the basic FD-TD/feedback algorithm. The FD-TD forward-scattering code calculates the pulse response of a trial target shape subjected to plane-wave illumination. The pulse response computed by FD-TD at the observation point is then compared with the measured pulse response, and an error signal is generated. This error signal is fed into an optimization routine which perturbs the trial target shape in a way that reduces the difference between the FD-TD trial pulse response and the measured pulse response. Target reconstruction is achieved by iterating through the feedback loop and reducing the error between the FD-TD trial response and the measured pulse response in the least-squares sense.

That is, we minimize error term given by:

$$\sum_{n=1}^{N} |E_{i_{\text{measured}}} - E_{i_{\text{FD-TD}}}| \tag{1}$$

where

$E_{i_{\text{measured}}}$: set of measured samples of the pulse waveform at the observation point;

$E_{i_{\text{FD-TD}}}$: set of time samples of the pulse generated by the forward-scattering FD-TD element.

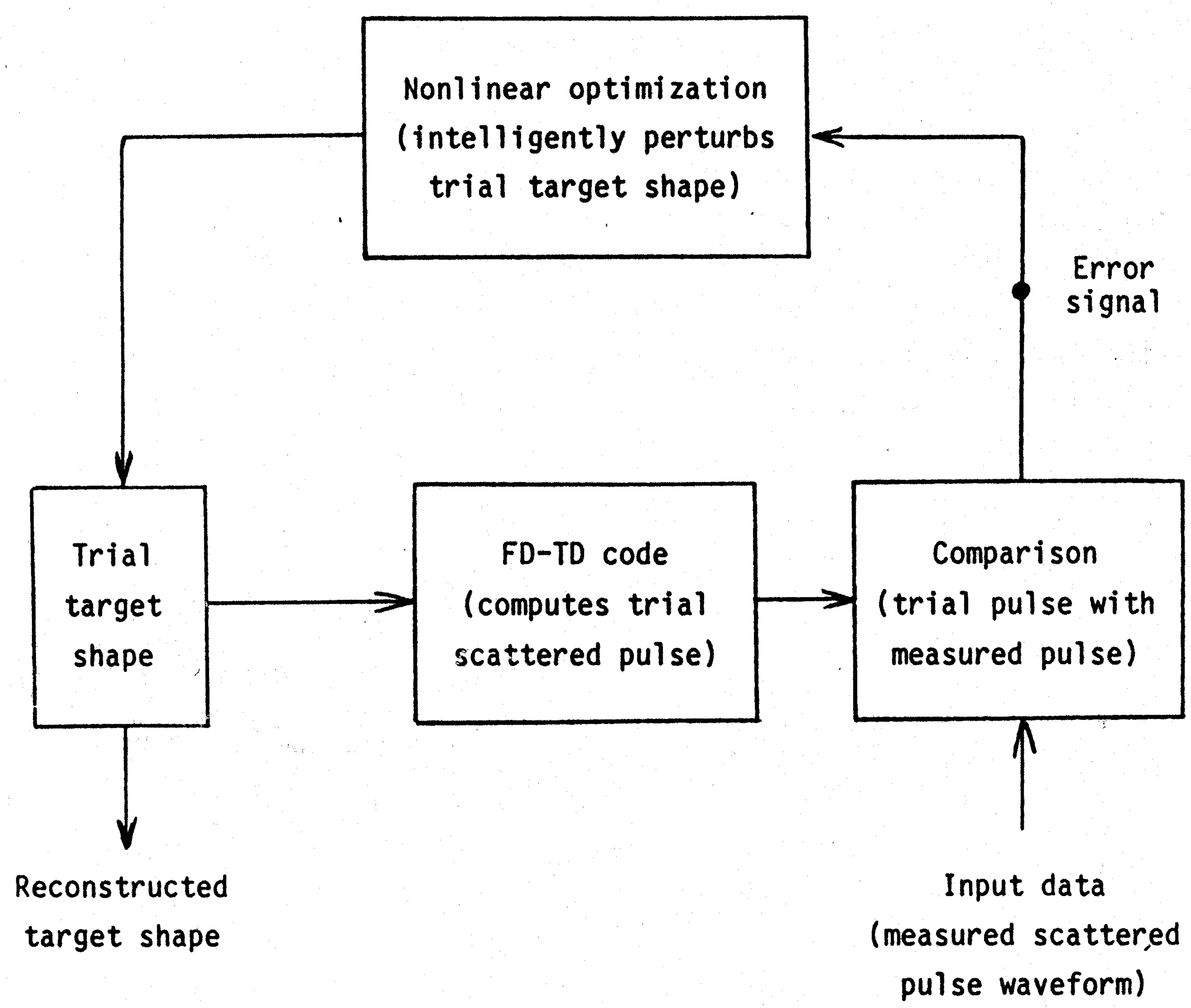

Figure 1. Block diagram of FD-TD feedback method for inverse scattering.

IV. CAUSALITY LOCUS

One of the most important features of the FD-TD/feedback approach is the exploitation of causality. Figure 2 shows a diagram of causality in two-dimensional free space. At time $t = 0$, a wavefront coming up from the bottom of the figure passes through the observation point, $\bar{r}_{obs}$. At a subsequent time t, the locus of all points where a point scatterer could be detected at robs is a parabola such that the distance $Y_{scat} + R_{scat} = ct$, where t is the time that has elapsed since the wavefront passed through $\bar{r}_{obs}$.

The significance of the causality locus is illustrated in Fig. 3a, which shows a triangular target illuminated by a plane wave. The causality locus is sweeping up the figure, and eventually strikes what we call the "first point". The first point is simply the very first point on the target that an observer located at $\bar{r}_{obs}$ can detect. After locating the first point, we reconstruct the target sequentially in time as the causality locus moves across the target. The advantage of exploiting causality is that the only portion of the target that can be reconstructed at a given time is the portion located beneath the causality locus. This reduces the complexity of reconstruction since only a portion of the target is being reconstructed at each iteration.

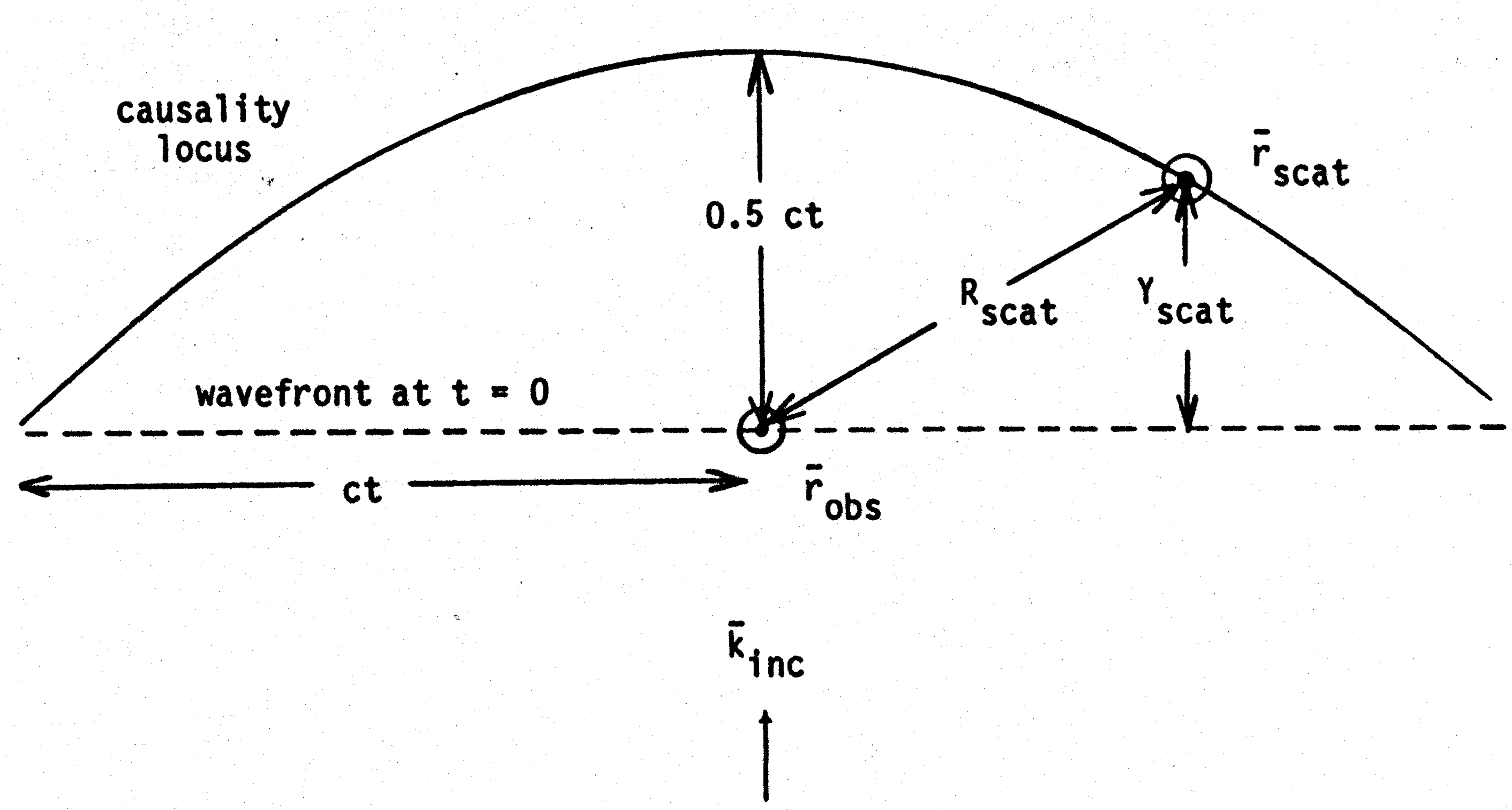

Figure 2. Free-space causality locus at time $= t$ ($ct = Y_{scat} + R_{scat} =$ constant).

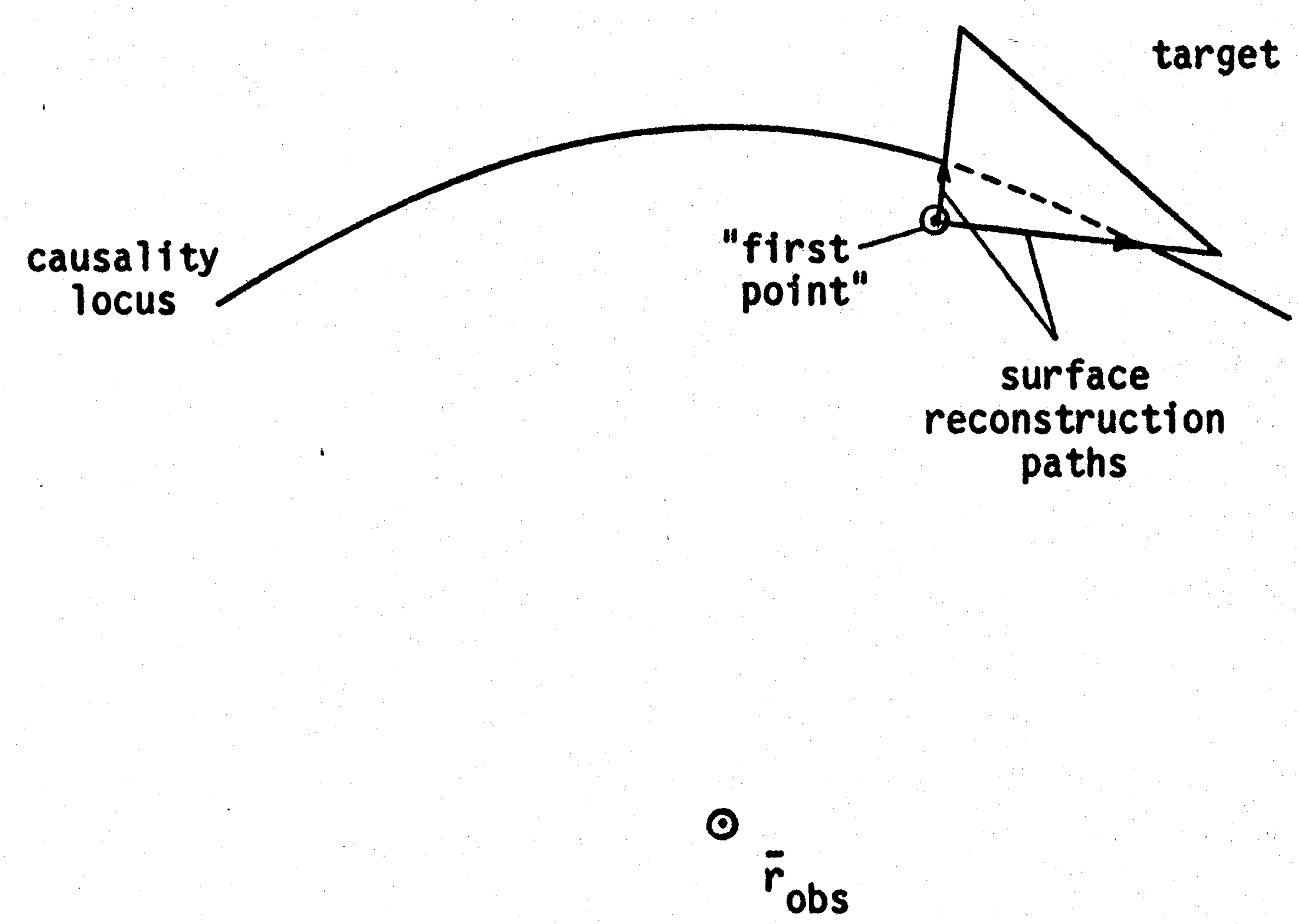

(A)

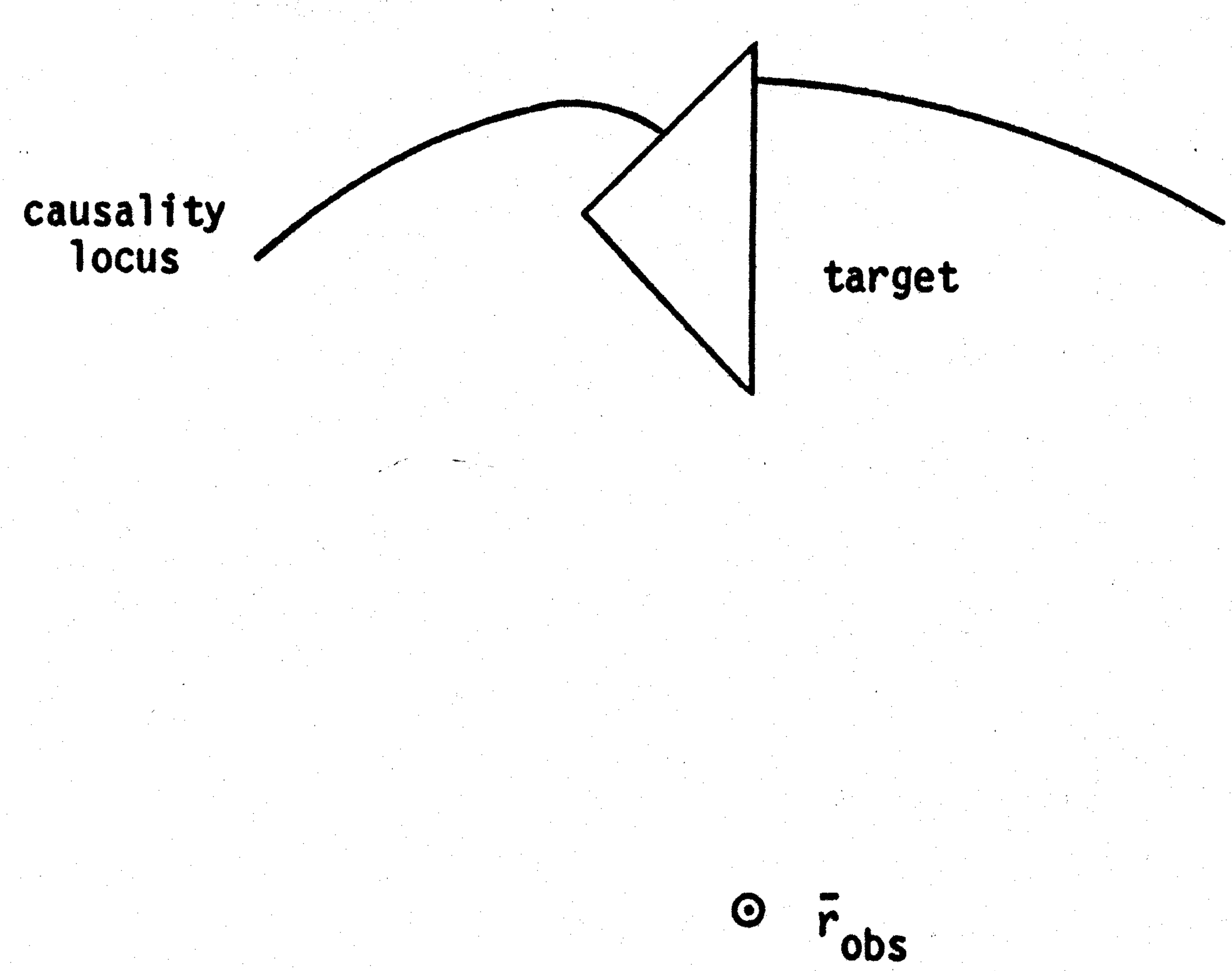

(B)

Figure 3. Free-space causality locus intersecting a target. (A) "First point" and surface reconstruction paths; (B) Causality locus distortion due to shadowing.

A complication arises, however, if we attempt target reconstruction in shadow regions or in reentrant regions. Here, as the causality locus interacts with the target, it no longer retains its free-space parabolic shape, but becomes distorted. An example of causality locus distortion due to shadowing is illustrated in Fig. 3b. Figure 3b shows that to an observer located at $\bar{r}_{obs}$, the top side of the triangle is in a shadow region, that is, there are no direct ray paths from points in this region to $\bar{r}_{obs}$. Thus, additional propagation delay is involved in sensing scattering from this region as energy diffracts back around the target along indirect ray paths. The causality locus in this region folds back toward $\bar{r}_{obs}$ to account for the additional propagation delay. Similar causality locus distortion is noted in cavities and other reentrant regions where no direct ray paths to $\bar{r}_{obs}$ exist. Causality locus distortion must be taken into account by the target reconstruction algorithm to avoid complete divergence of the actual and reconstructed target shapes.

V. APPROACH 1: RECONSTRUCTION OF CONDUCTING TARGETS USING CONTOUR FOLLOWING

Figure 4 illustrates how conducting target shapes can be reconstructed using contour following. In this figure, we assume that the causality locus previously struck the vertex of a triangular target; and, as the locus swept up the target, the portions of the triangle from the first point to points A and A' were successfully reconstructed. We must now continue target reconstruction from points A and A'. Since the FD-TD grid has discretized the space in which the trial target is embedded, we have only a finite number of guesses for the manner in which the surface contour can vary adjacent to A and A'. That is, we can continue reconstruction only in discrete jumps that are bounded by the resolution of the FD-TD grid. As Fig. 4 shows, to continue target reconstruction from point A, we have four possible surface paths that need to be investigated.

The optimization routine now sequentially assigns high conductivity values to each of the four possible surface paths from point A, and in turn, the FD-TD element computes the scattered pulse response for each of the four trial paths. The algorithm then compares the four trial pulse responses with the measured data, and selects the path that produces a pulse response best fitting the measured data in the least-squares sense. This process is now repeated using point A' as the base from which to launch the target surface perturbations. In this manner, by alternating between the lefthand and righthand points generated in the previous iteration, the target surface is reconstructed synchronously as the causality locus moves across the target.

Figure 5a shows four examples of two-dimensional conducting targets successfully reconstructed using the contour-following method in the absence of noise (along with associated running times on the VAX 11/780). Each target is about 0.5 λ_0 wide. The observation point is 1.5 λ_0 from the front of each target and the incident illumination is a TM-polarized carrier burst 5 cycles long. The "measured" scattered electric field waveform at the observation point was numerically generated by a forward-scattering FD-TD code having the same 0.1 λ_0 spatial resolution as the FD-TD/feedback code. Figure 5b shows a similar reconstruction (and associated VAX time) of a 0.6 λ_0 triangular target from a distance of 15 λ_0. In both Figs. 5a and 5b, the target size and observation distance are shown to scale.

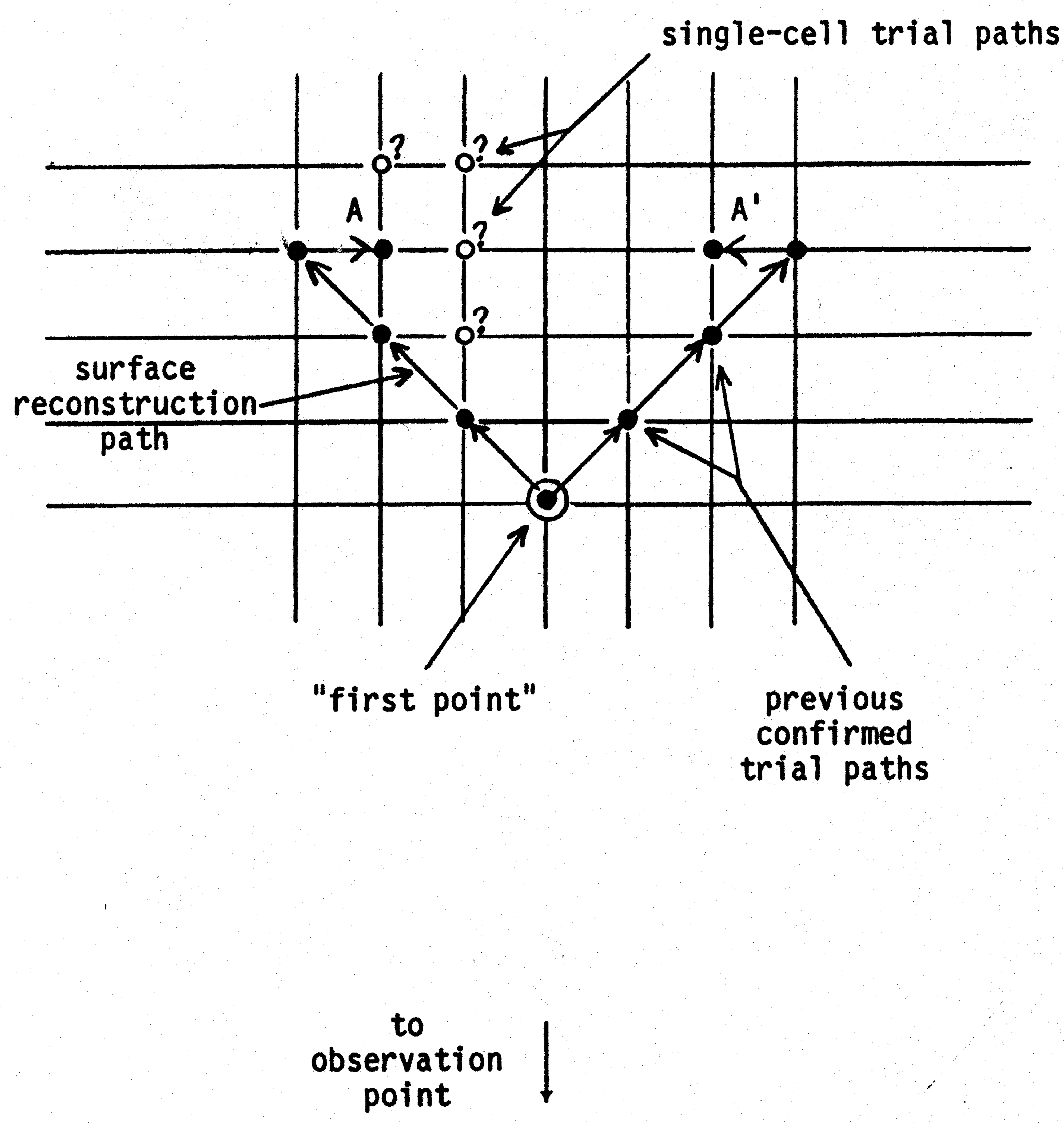

Figure 4. Typical target surface perturbation.

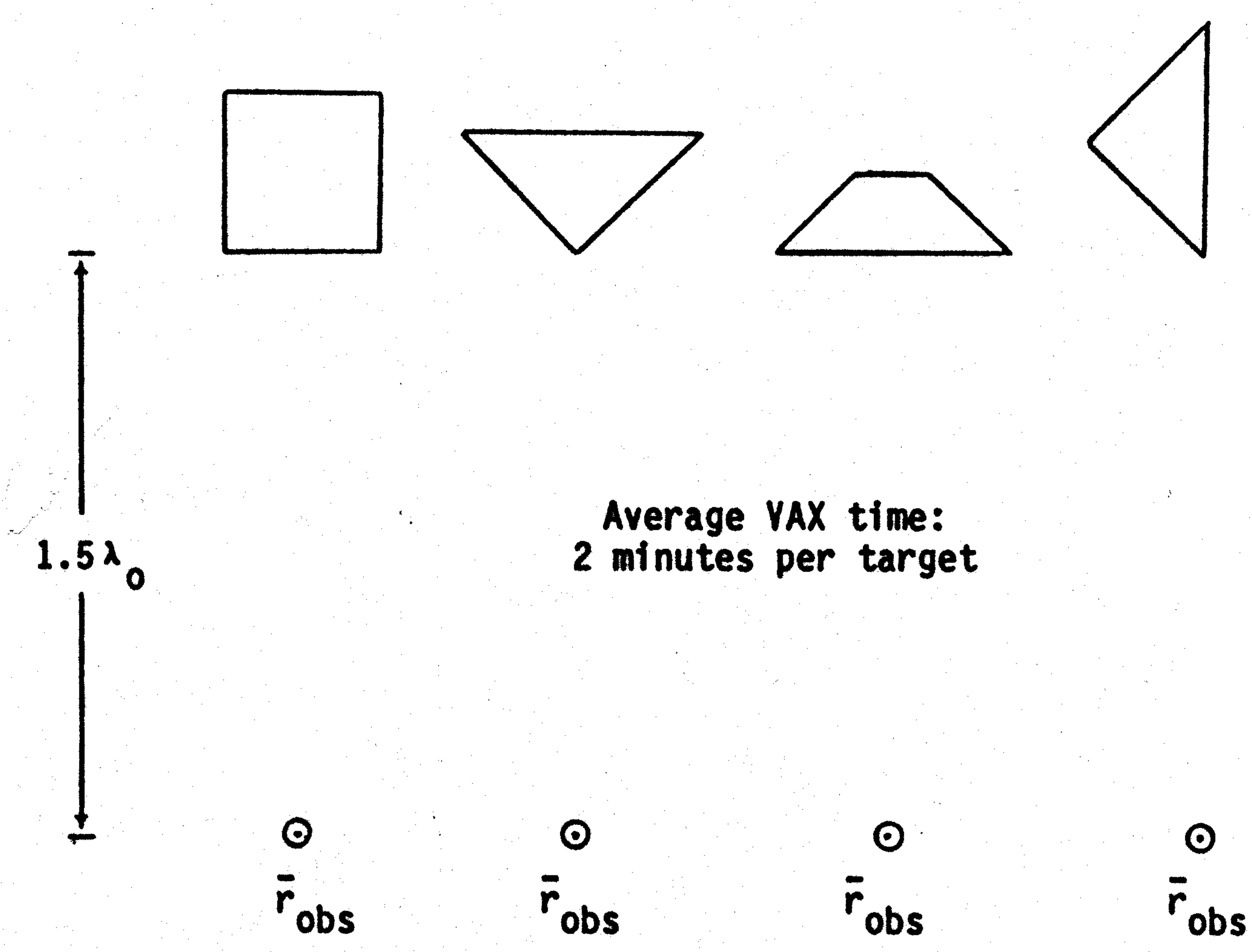

(A)

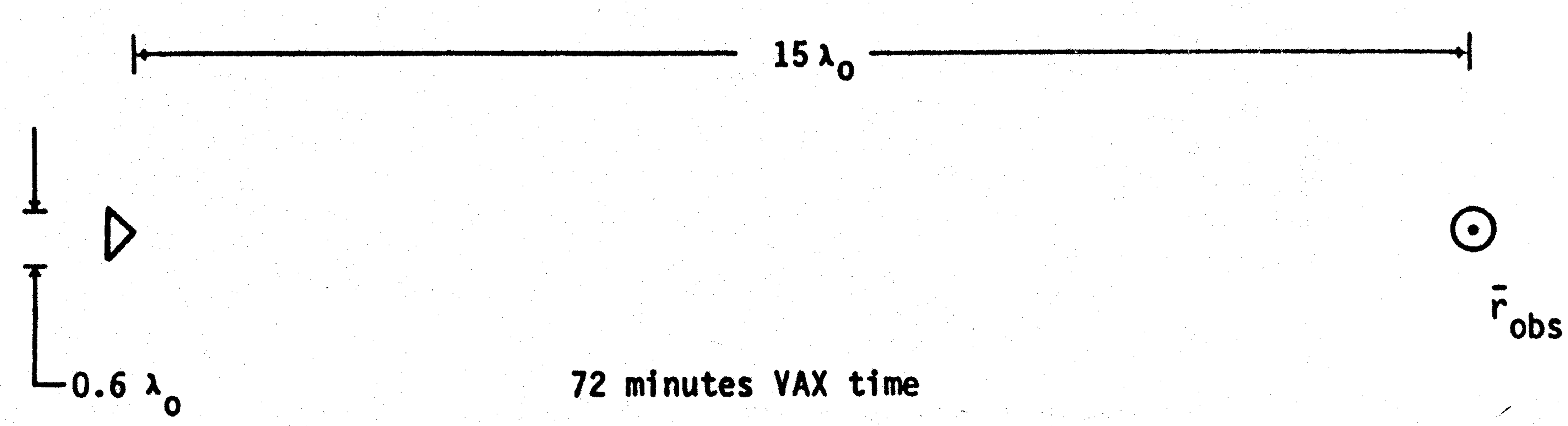

(B)

Figure 5. Examples of target reconstruction using contour following. (A) Observation point close to target; (B) Observation point relatively far from target.

VI. APPROACH 2: GRADIENT METHOD (LAYER RECONSTRUCTION)

Although contour following is easy to apply to the reconstruction of two-dimensional convex targets, it has limitations in that: a) it is awkward to apply to targets having reentrant features; and b) it is not easily extended to target reconstruction in three dimensions. We now describe an alternate procedure for target reconstruction that does not share these deficiencies. This procedure can be applied if the target does not have deep reentrant features, such as cavities, so that the causality locus is not excessively distorted from its parabolic free-space shape. In the absence of excessive causality locus distortion, we can reconstruct the target as a series of parallel layers if the observation point is sufficiently far from the front of the target so that the causality locus can be approximated by a straight line across the width of the target. The thickness of each reconstructed layer is then determined by the position of the causality locus with respect to the previously reconstructed layer. In layer reconstruction, the optimization program must determine the width of each layer and its orientation with respect to the layer to which it is to be attached.

Figure 6 shows an example of layer reconstruction. The shaded rectangular region in Fig. 6a represents the portion of the target that has already been reconstructed. The causality locus has moved beyond the existing reconstruction to the position shown in the figure. We must now attach another layer to the existing reconstruction. Figures 6b to 6d show three possible reconstruction choices which are indicated by the dotted lines. To indicate the orientation of the trial layer with respect to the layer to which it is to be attached, we create a left/right shift coordinate system denoted from now on by L and R. For example, in Fig. 6b the width of the trial layer is identical to the previously reconstructed layer to which it is attached. It is shifted neither to the left or right, therefore $L = 0$ and $R = 0$. In Fig. 6c, both the left and right shift is one cell, therefore $L = 1$ and $R = 1$. In Fig. 6d, the left shift is zero and the right shift is two cells, hence $L = 0$ and $R = 2$. Obviously, there are many choices for the new layer other than the three illustrated. The best choice or global error minimum could be obtained by an exhaustive, systematic exploration of the entire L/R space. However, to quickly find a layer choice which provides at least a local error minimum, we use a gradient method as shown in Fig. 7.

To obtain a choice for the new layer, we begin by calculating the trial pulse responses of the arbitrarily located group of 4 left/right shift points arranged in the square block-like pattern shown in Fig. 7. The least-square errors between the measured pulse response and the 4 trial pulse responses, denoted by E_1 to E_4, are calculated and recorded alongside each L/R point. To calculate the direction we should proceed in L/R space to minimize the error, we obtain a numerical approximation to the negative value of the error gradient vector using

$$-\nabla_{\text{error}} = [E_1 - E_2 + E_4 - E_3]\hat{R} + [E_4 - E_1 + E_3 - E_2]\hat{L} \tag{2}$$

which is indicated by the arrow in Fig. 7. We now follow this direction into one of the eight neighboring blocks in L/R space and recalculate the error gradient vector. In this manner, we are able to locate an approximate region in the L/R space where the least-square error is at worst a local minimum. This approach is advantageous in that it simultaneously determines the width of the new layer and its left/right orientation with respect to the previously reconstructed layer.

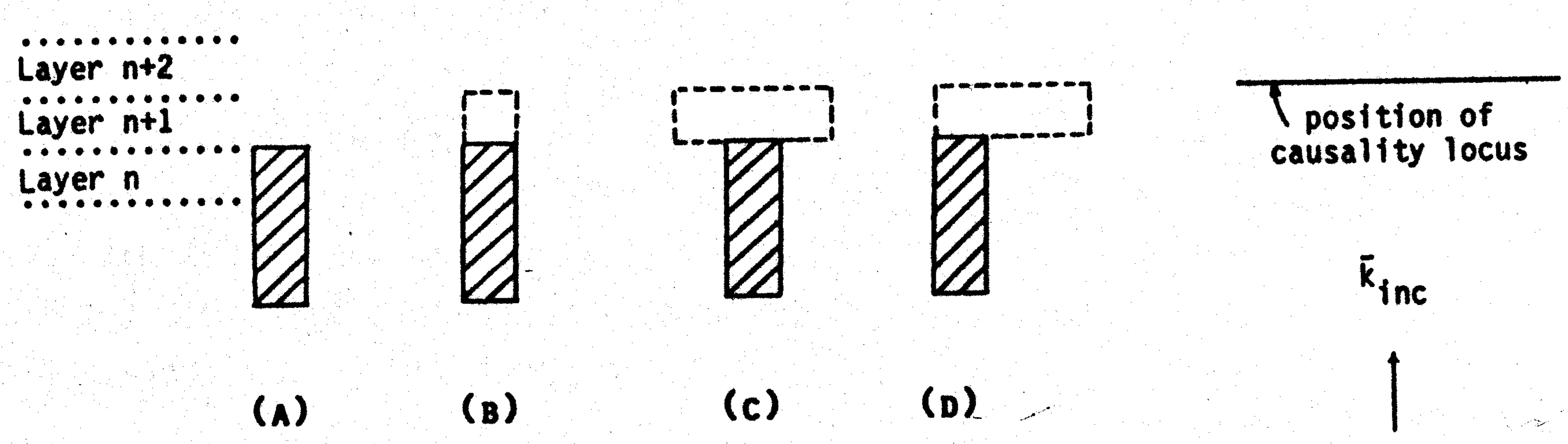

Figure 6. Example of reconstruction trials using the layer method. (A) Portion of target already reconstructed; (B) Trial layer having $L = 0$ and $R = 1$; (C) Trial layer having $L = 1$ and $R = 1$; (D) Trial layer having $L = 1$ and $R = 2$.

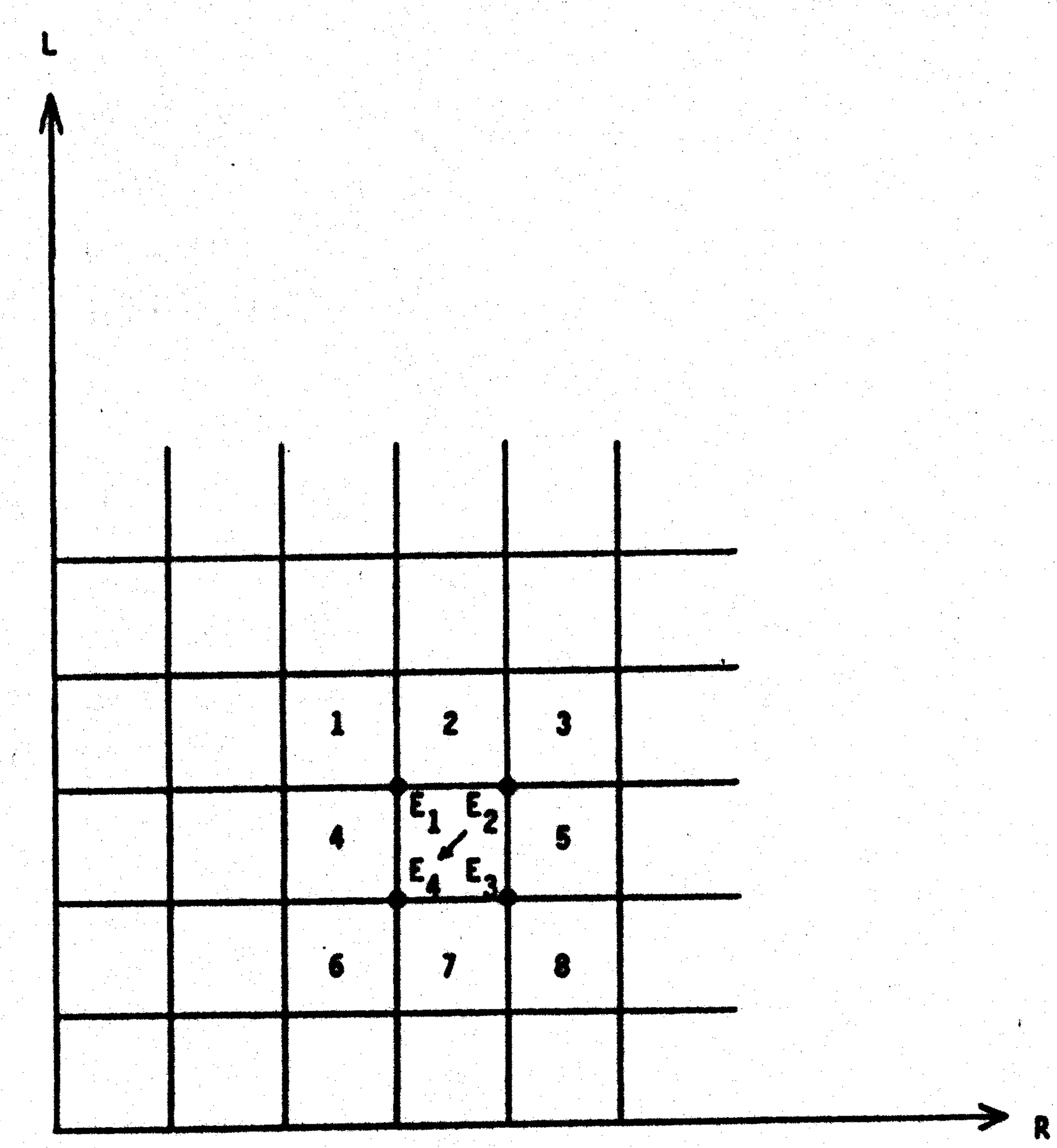

Figure 7. Error gradient study in Left/Right shift space.

Two examples of targets that were successfully reconstructed in the absence of noise using this technique are shown in Figure 8, along with the associated VAX times. The triangle is 0.03 λ_0 tip-to-base, and is a nearly perfect conductor. The J-shaped target is 0.06 λ_0 front-to-back, and is a homogeneous dielectric with $\epsilon_r = 2.1$. For both targets, the observation point is located 0.15 λ_0 from the front of the target, and the incident wave is a TM-polarized carrier burst 5 cycles long. The "measured" scattered electric field waveform at the observation point was numerically generated by a forward-scattering FD-TD code having the same 0.01 λ_0. spatial resolution as the FD-TD/feedback code.

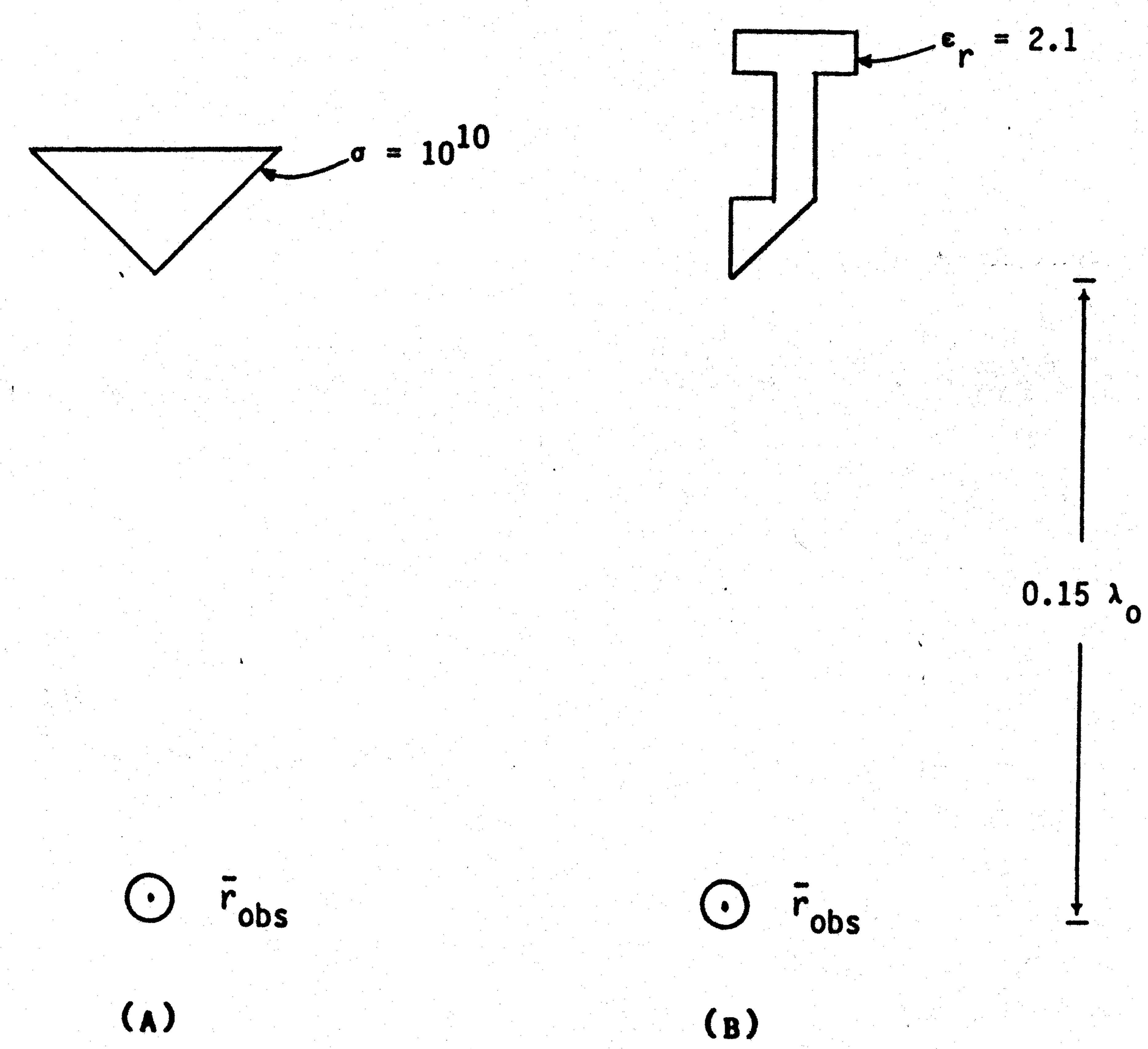

Figure 8. Examples of target reconstruction using gradient (layer) method in the absence of noise. (A) Conducting triangle, VAX time = 2.3 minutes; (B) Dielectric "J", VAX time = 3.5 minutes,

Figure 9 shows an example of a gradient study that was done on the dielectric J of Fig. 8b in order to reconstruct the bottom portion of the crossbar of the J. The crossbar is 3 cells wide and extends 1 cell to the left and right of the vertical portion of the J located immediately underneath it. Figure 9 shows as heavy dots the trial L/R shift points, and arrows representing the corresponding least-square error gradient vectors. Figure 9 shows that no matter where we started in the L/R shift space, the gradient search moved toward the line that passes through the points $(L = 3, R = -1), (L = 2, R = 0), (L = 1, R = 1)$, etc. The sum of $L + R$ along this line equals 2, exactly the number of cells that the new layer is to be extended beyond the old layer. The points on this line correspond to the points of minimum least-square error in the neighborhood a round the line. To quickly proceed to the correct choice, $(L = 1, R = 1)$, we simply perform a search along this line. A consequence of using only the scattered electric field at a single point as the input data is that there is an ambiguity in target reconstruction, as shown in Fig. 10. Both versions of the dielectric J produce the same scattered electric field pulse waveform at the observation point. The target on the left in this figure is generated by rotating the original target $180°$ around the axis indicated by the dotted line, which passes through the observation point.

VII. GRADIENT RECONSTRUCTION WITH NOISY DATA

When the measured pulse data is contaminated with noise, it may be difficult to initially determine the correct L/R choice for a given layer. For example, layers of equal width, as illustrated by the two choices in Figs. 6c and 6d, may initially produce a similar scattered pulse response at the observation point. One way to determine the best choice for this layer is temporarily accept both choices as correct, and then build additional layers on each of the two choices until the incorrect choice becomes apparent by producing a large error signal.

This technique is illustrated in Fig. 11 using as an example the reconstruction shown in Fig. 6. The known L/R shift in layer n is shown in the bottom of Fig. 11 as the black dot at the origin of the L/R coordinate system. The two ambiguous choices for layer $n + 1$, namely $(L = 0, R = 2)$ and $(L = 1, R = 1)$, are shown as dots in layer $n + 1$. These two choices for layer $n + 1$ are connected by solid lines to the point $(L = 0, R = 0)$ in layer n, the solid lines indicating that each choice is physically connected to a layer n as shown in Figs. 6c and 6d. For each of the two choices in layer $n + 1$, we now construct layer $n + 2$. For example, Fig. 11 shows three sample best choices for layer $n + 2$ that correspond to the choice $(L = 0, R = 2)$ in layer $n + 1$. These choices are obtained by using the gradient method to locate the approximate region of least error in the $n + 2$ layer L/R shift space. We then systematically explore this region to obtain the three best L/R shift points. The figure generated by this type of construction resembles a tree, where the branches consist of the solid lines that extend from one layer to the next indicating the physical connection between layers. A tree can also be constructed for the choice $(L = 1, R = 1)$ in layer $n + 1$. That is, we complete the construction of this tree by determining the three best L/R shift choices for layer $n+2$. With the two trees completed through layer $n+2$, we can now determine the best choice for layer $n+1$ by adding the total least-square error as calculated by Equation (1) for each of the trees as the causality locus moves to the top edge of layer $n+2$. The best choice for layer $n+1$ is determined by choosing the tree that produces the smallest total error. In this manner, the L/R choice for a given layer is made one layer behind the actual position of the causality locus. If the noise level increases, more trees can be constructed and tested for error, and the L/R choice for a given layer can be delayed even further behind the causality locus position.

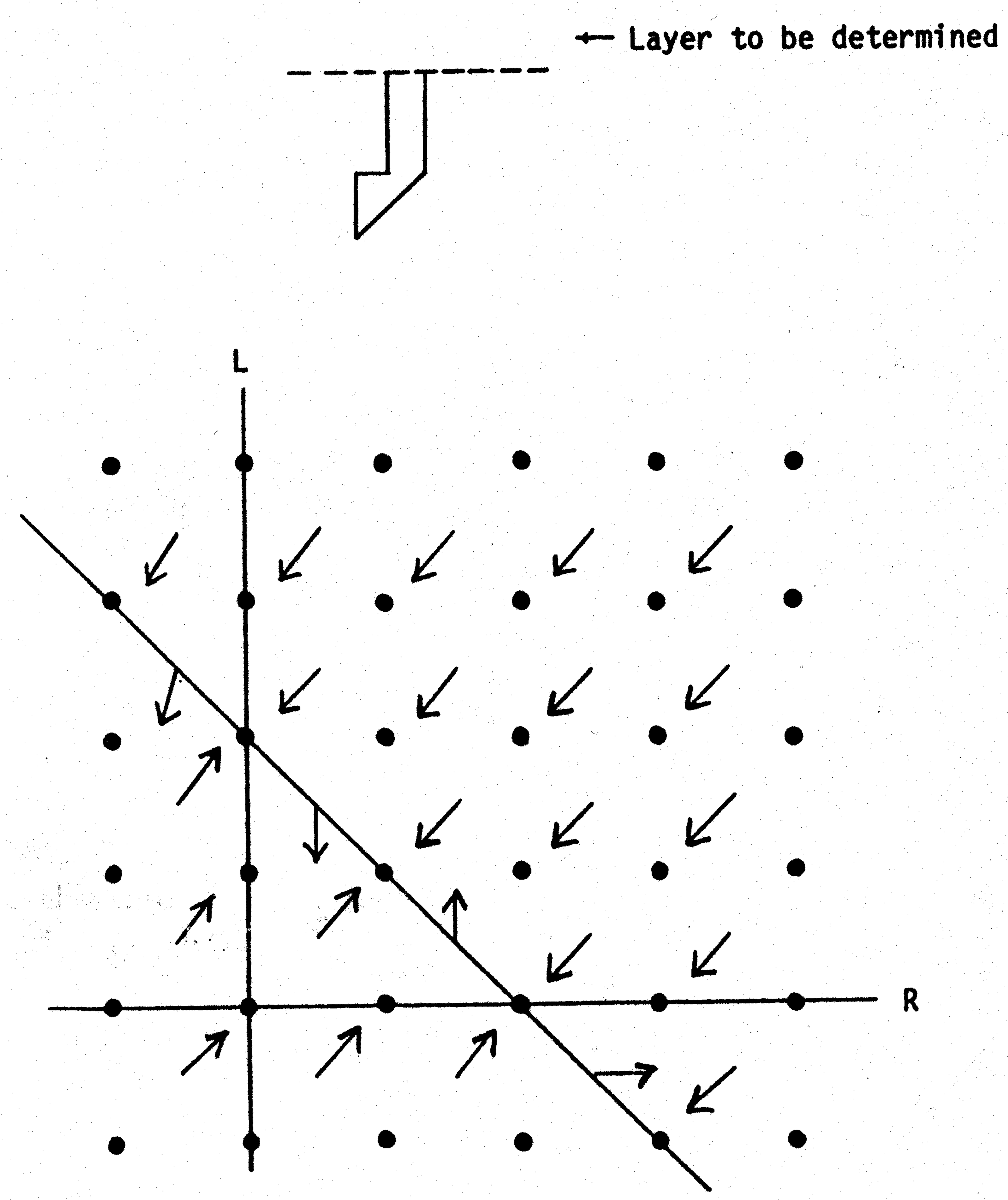

Figure 9. Sample error gradient study for the dielectric "J".

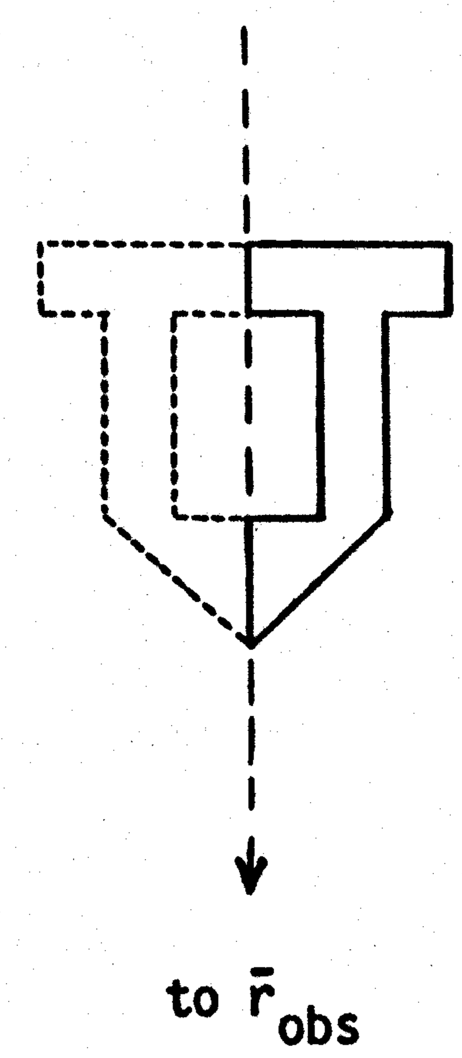

Figure 10. Target reconstruction ambiguity.

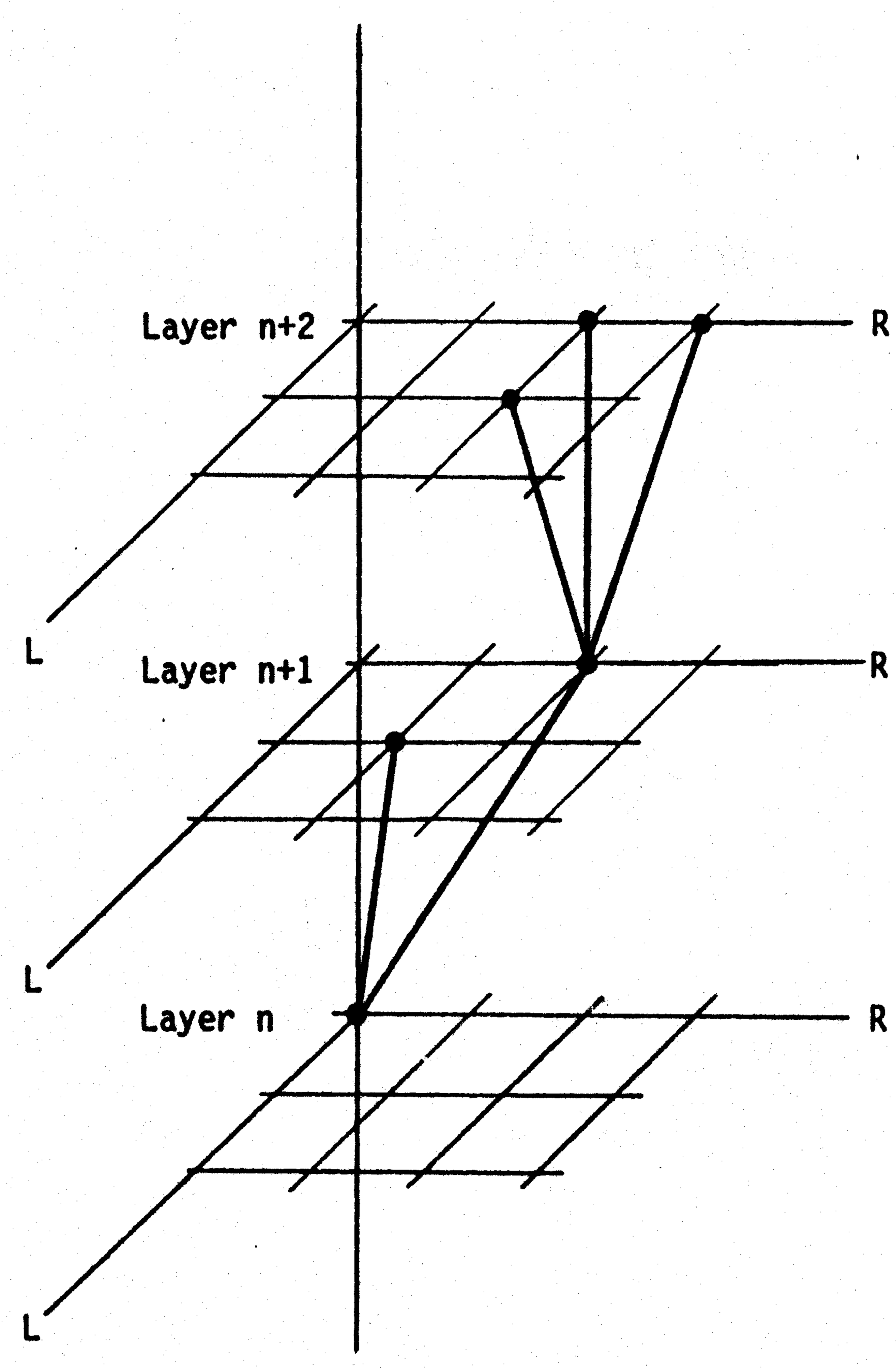

Figure 11. Reconstruction tree.

VIII. EXAMPLES OF TARGET RECONSTRUCTION WITH NOISY DATA USING THE GRADIENT METHOD

A number of numerical experiments have been performed to determine the effect of additive zero-mean Gaussian noise upon target reconstruction using the gradient method. Figures 12 and 13 show the probability of exact reconstruction versus signal-to-noise (S/N) ratio for the conducting triangle and dielectric J targets of Fig. 8. Figure 14 shows sample reconstructions of these targets with $S/N =$ 20dB, 25dB, and 30dB, with the reconstructed target shape shown superimposed on the exact target shape (indicated by the shading). In Figs. 12 to 14, the target size, observation point location, and incident wave are the same as that of Fig. 8. The signal power level used to calculate the signal-to-noise ratio is taken as the root-mean-square value of the scattered electric field pulse waveform at the observation point from the time that the scattered pulse first arrives until the causality locus moves about one-half target length beyond the back of the target. The gradient search for each new layer starts at the origin of the L/R coordinate system. The L/R choice for each layer is delayed by building a tree with three branches that extends into the next layer. Target reconstruction is terminated when adding additional layers beyond a certain point produces more error than terminating the target reconstruction at that point.

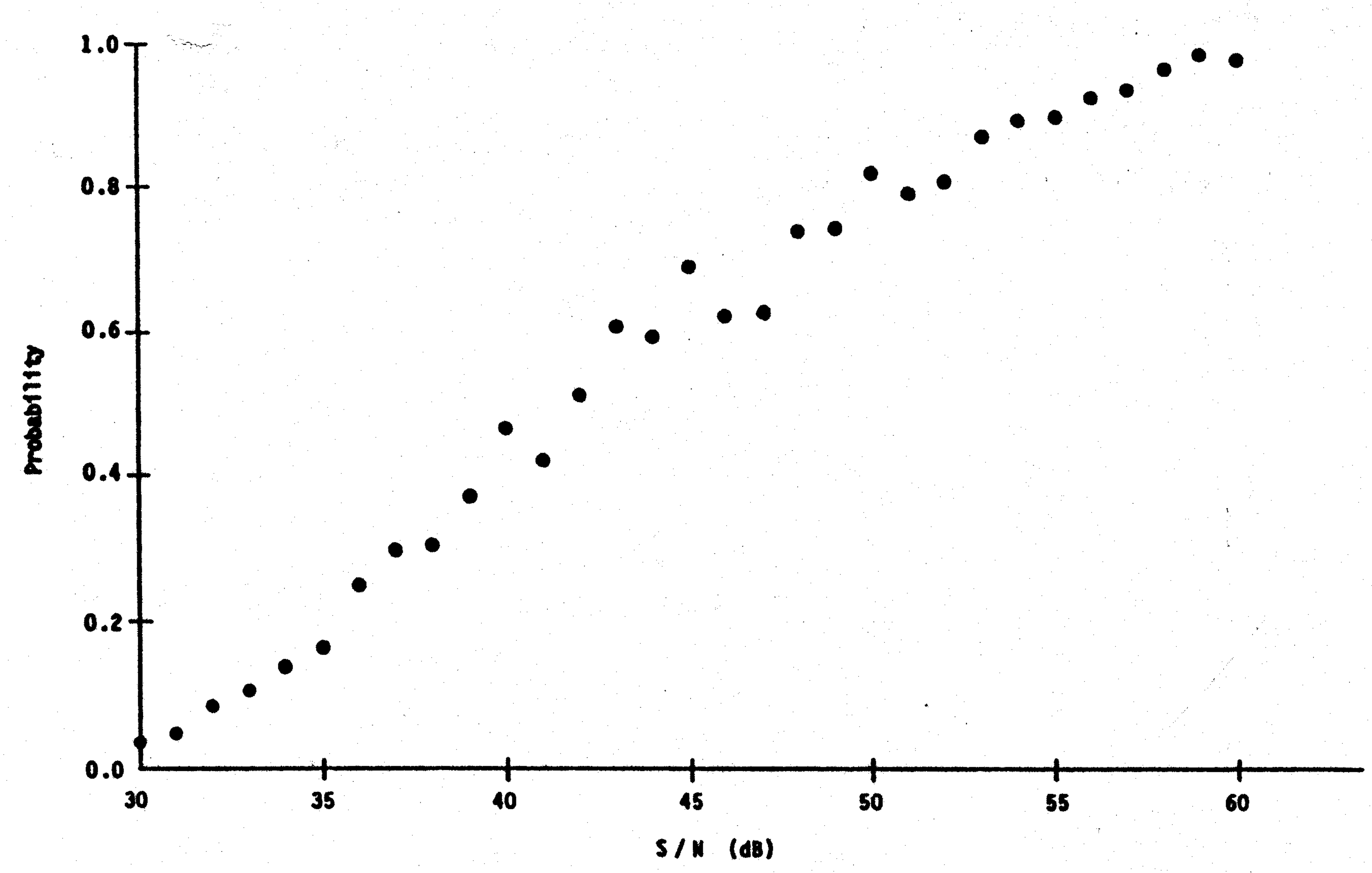

Figure 12. Probability of exact reconstruction vs. signal-to-noise ratio for the conducting triangle target of Fig. 8, as evidenced in 200 reconstructions.

Figures 12 and 13 show that we need large signal-to-noise ratios exceeding 55dB to have a 0.9 probability or higher of exact reconstruction. However, Figure 14 shows that even at low signal-to-noise ratios, the reconstructed target still retains many of the distinguishing features of the original target. This indicates that the reconstruction process is quite robust relative to noise, a necessary characteristic of well-posedness.

IX. CONCLUSION

This paper introduced two iterative techniques for the reconstruction of homogeneous target shapes in two dimensions. The techniques are based on using a nonlinear optimization routine combined in a numerical feedback loop with a finite-difference time-domain representation for the electromagnetic fields. This approach has been used to reconstruct both convex perfectly conducting targets and homogeneous dielectric targets. The input data to both algarithm consists of only the TM scattered electric field pulse waveform observed at a single point in the near field. Work continues in a number of different areas to extend the capabilities of the FD-TD/feedback technique for inverse scattering. For example, the feasibility of true far-field reconstruction of homogeneous two-dimensional targets using the scattered pulse observed at only a single look angle is being explored. Another avenue of research involves improving the robustness of the layer reconstruction method with respect to noise performance by modifying the nonlinear optimization routine to retain additional possible trial guesses for layer L/R coordinates for longer periods before rejection. Using the terminology of section VII, this would expand the growth of the decision trees by developing more branches, letting them grow into additional layers of the target, and then pruning the ones that ultimately develop large errors.

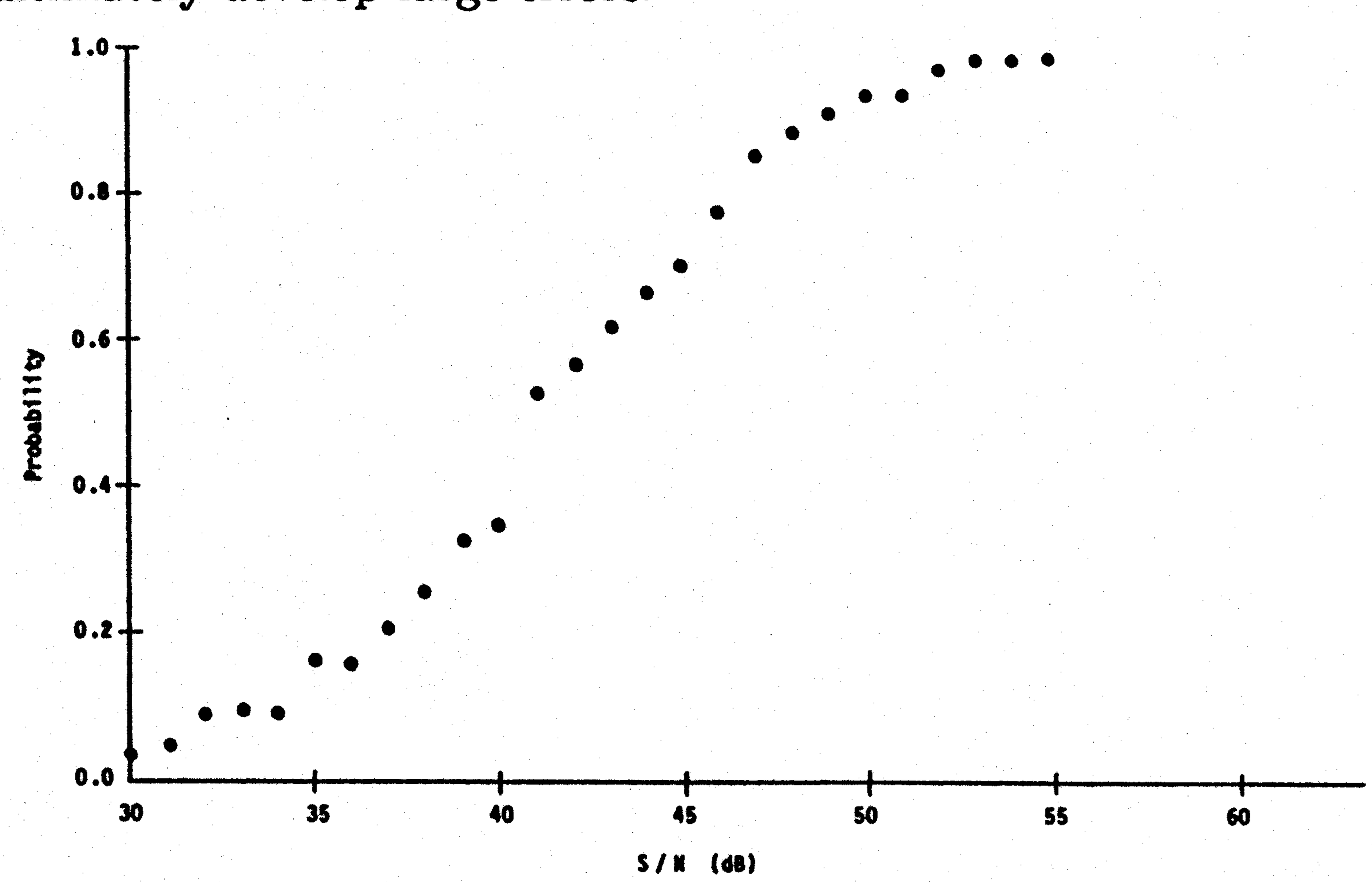

Figure 13. Probability of exact reconstruction vs. signal-to-noise ratio for the dielectric "J" target of Fig. 8, as evidenced in 200 reconstructions.

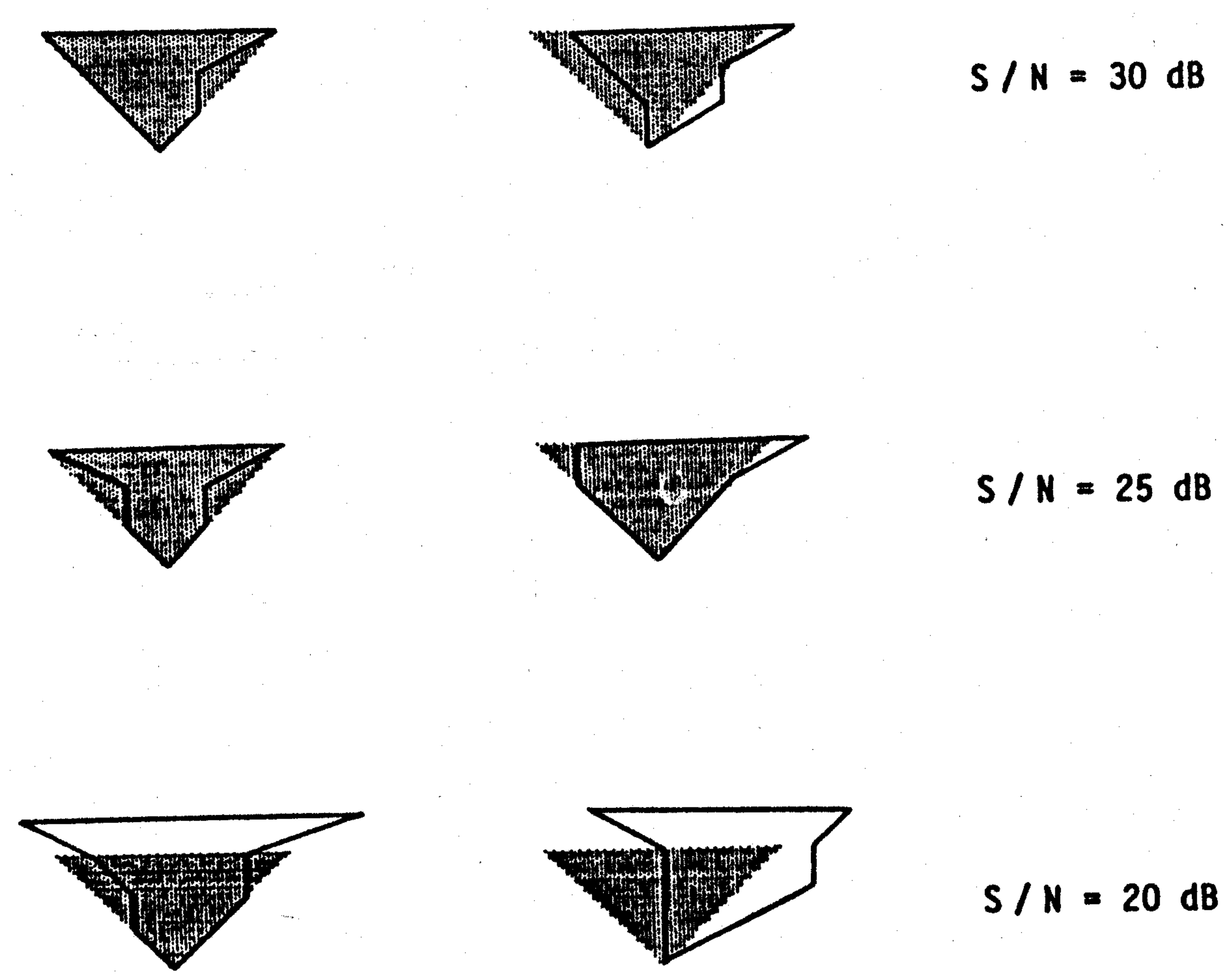

(A)

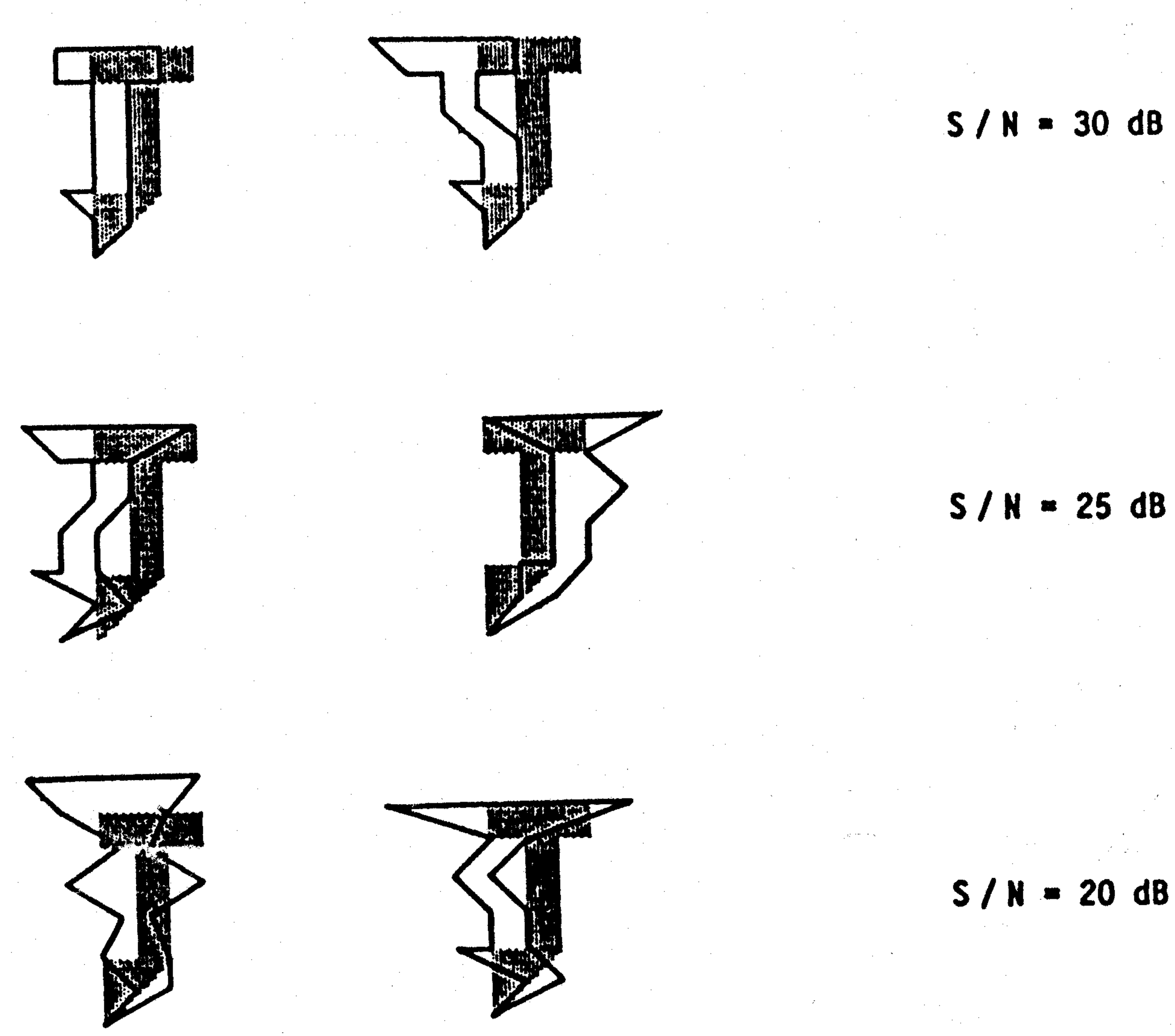

(B)

Figure 14. Sample reconstructions at low signal-to-noise ratios. (A) Conducting triangle target of Fig. 8, average VAX time = 9 minutes; (B) Dielectric "J" target of Fig. 8, average VAX time = 14 minutes.

Work is also ongoing in reconstructing homogeneous two-dimensional targets having multiple first-points. Targets of this type may have reentrant features in the lit region, or may consist of two closely spaced, but distinct shapes not physically connected together. Additional extensions involve improvements in the optimization routines applicable to the discrete nature of the FD-TD grid using, for example, combinatorial optimization techniques. Conversely, new conformal curved surface FD-TD models [15], which effectively remove the stepped-surface nature of the FD-TD trial target, may be used in the forward-scattering element to permit application of conventional variable metric and conjugate gradient optimization techniques in the feedback element.

Finally, the feasibility of extending the layer reconstruction method to three dimensions will be explored. Here, a four-dimensional left/right/up/down shift space would be set up, in a natural extension of the left/right space used for two-dimensional reconstructions. Now, target layers would consist of rectangular sheets whose boundaries would be determined by a gradient search strategy analogous to that of section VI. Reconstruction ambiguities and increased requirements for measured data, along with substantially increased computer time needed to implement iterations of the three-dimensional forward-scattering FD-TD code, are expected to be major concerns here.

ACKNOWLEDGMENTS

This work was supported in part by NASA Lewis Research Center under grant No. NAG 3-635.

The Editor thanks C. Lee, D. Lesselier, W. Tabbara, and A. G. Tijhuis for reviewing the paper.

REFERENCES

1. Chaudhuri, S. K., K. R. Umashankar, and A. Taflove, "Finite-difference time-domain formulation of an inverse scattering scheme for remote sensing of inhomogeneous lossy layered media," *Proc. National Radio Science Meeting (URSI),* Vancouver, B.C., p. 150, June 1985.
2. Umashankar, K., S. Chaudhuri, and A. Taflove, "Finite-difference time-domain formulation of an inverse scattering scheme for remote sensing of inhomogeneous lossy layered media, Part I - One dimensional case," *J. of Electromagnetic Waves and Applica.,* to appear, 1994.
3. Fawcett, J., "Two-dimensional velocity inversion of the acoustic wave equation," *Wave Motion,* Vol. 7, No. 6, 503–513, Nov. 1985.
4. Gauthier, O., J. Virieux, and A. Tarantola, "Two-dimensional nonlinear inversion of seismic waveforms: numerical results," *Geophysics,* Vol. 51, No. 7, 1387–1403, July 1986.
5. Bennett, C. L., "Time domain inverse scattering," *IEEE Trans. Antennas Propagat.,* Vol. AP-29, No. 2, 213–219, March 1981.
6. Bolomey, J. C., D. Lesselier, C. Pichot, and W. Tabbara, "Spectral and time domain approaches to some inverse scattering problems," *IEEE Trans. Antennas Propagat.,* Vol. AP-29, No. 2, 206–212, March 1981.

7. Tijhuis, A. G., "Iterative determination of permittivity and conductivity profiles of a dielectric slab in the time domain," *IEEE Trans. Antennas Propagat.*, Vol. AP-29, No. 2, 239–245, March 1981.
8. Miller, E. K., and J. A. Landt, "Direct time domain techniques for transient radiation and scattering from wires," *Proc. IEEE,* Vol. 68, No. 11, 1396–1423, Nov. 1980.
9. Yee, K. S., "Numerical solution of initial boundary value problems involving Maxwell's equations in isotropic media," *IEEE Trans. Antennas Propagat.*, Vol. AP-14, 302–307, May 1966.
10. Engquist, B., and A. Majda, "Radiation boundary conditions for acoustic and elastic wave calculations," *Comm. Pure Appl. Math.*, Vol. 32, 313–357, 1979.
11. Bayliss, A., and E. Turkel, "Radiation boundary conditions for wave-like equations," *Comm. Pure Appl. Math.*, Vol. 33, 707–725, 1980.
12. Mur, G., "Absorbing boundary conditions for the finite-difference approximation of the time-domain electromagnetic field equations," *IEEE Trans. Electromagn. Compat.*, Vol. EMC-23, 1073–1077, Nov. 1981.
13. Umashankar, K. R., and A. Taflove, "A novel method to analyze electromagnetic scattering of complex objects," *IEEE Trans. Electromagn. Compat.*, Vol. EMC-24, 397–405, Nov. 1982.
14. Taflove, A., and K. R. Umashankar, "The finite-difference time-domain (FD-TD) method for electromagnetic scattering and interaction problems," *J. Electromagnetic Waves and Applica.*, Vol. 1, 1987.
15. Jurgens, T. G., A. Taflove, and K. R. Umashankar, "Conformal FD-TD modeling of objects with smooth curved surfaces," *Proc. National Radio Science Meeting (URSI),* Blacksburg, Virginia, June 1987.

Mark Strickel was born in Chicago, Illinois, on August 13, 1955. He received the B.S. degree from Illinois Institute of Technology, in 1983 and M.S. and Ph.D. degrees in Electrical Engineering from Northwestern University, Evanston, Illinois in 1984 and 1989, respectively. From 1982 to 1984, he was a staff member in the Electronics Division, IIT Research Institute, Chicago, Illinois. From 1988 to 1990, he was a staff member of the Institutional Financial Features and Options Divisions of Drexel Burnham Lambert. He is currently with Rand Financial Services, Chicago, Illinois. Dr. Strickel is a member of Eta Kappa Nu.

Allen Taflove was born in Chicago, Illinois, on June 14, 1949. He received the B.S., M.S., and Ph.D., degrees in Electrical Engineering from Northwestern University, Evanston, Illinois in 1971, 1972, and 1975, respectively. From 1975 to 1984, he was a staff member in the Electronics Division, IIT Research Institute, Chicago, Illinois. During 1984, he returned to Northwestern University where he is a Professor of Electrical Engineering and Computer Science. He has authored two text books. Dr. Taflove is a member of Tau Beta Pi, Eta Kappa Nu, Sigma Xi, URSI Commission B, The Electromagnetics Academy, and a Fellow of IEEE.

Korada Umashankar received the B.E. degree from Mysore University and M.E. degree from Indian Institute of Science, Bangalore, India and Ph.D. degree from University of Mississippi, all in Electrical Engineering. From 1975 to 1977 he was with faculty of University of Mississippi, from 1977 to 1979 with Airforce Weapons Lab., KAFB, Albuquerque and from 1979 to 1984 a staff member in the Electronics Division, IIT Research Institute, Chicago, Illinois. During 1984, he joined University of Illinois at Chicago where he is a Professor of Electrical Engineering and Computer Science. He has authored three text books. Dr. Umashankar is a member of Eta Kappa Nu, Sigma Xi, URSI Commission B, and a Senior member of IEEE.